

Nanomechanical z-shape folding of graphene on flat substrate



Chenglin Yi^a, Xiaoming Chen^a, Liuyang Zhang^b, Xianqiao Wang^{b,*},
Changhong Ke^{a,c,*}

^a Department of Mechanical Engineering, State University of New York at Binghamton, Binghamton, NY 13902, USA

^b College of Engineering, University of Georgia, Athens, GA 30602, USA

^c Materials Science and Engineering Program, State University of New York at Binghamton, Binghamton, NY 13902, USA

ARTICLE INFO

Article history:

Received 31 January 2016

Received in revised form 23 April 2016

Accepted 18 May 2016

Available online 24 May 2016

Keywords:

Graphene

Folding

Buckling

Origami

Atomic force microscopy

ABSTRACT

Graphene folding is an essential process in the design and manufacturing of graphene origami. Here we report the nanomechanical z-shape (accordion) folding of single graphene sheets on flat substrates by using atomic force microscopy techniques. The quantitative nanomechanical measurements in conjunction with nonlinear mechanics modeling and molecular dynamics simulations reveal that a reversible out-of-plane buckling delamination of graphene occurs in its early-stage folding process, which enables graphene to deform into a stable self-folded z-shape conformation. The research findings are useful to the study of active and controllable folding of graphene and in the pursuit of graphene origami with intricate geometries.

© 2016 Published by Elsevier Ltd.

1. Introduction

Graphene is a type of ultra-thin two-dimensional nanomaterial with extraordinary mechanical and electrical properties [1,2], and is considered an ideal building material for *origami* and *kirigami* [3–7]. Constructed through folding originally flat graphene sheets into a variety of sculptures, graphene origami is not only an artwork, but also promising for many engineering applications, such as energy storage, 3D optics, and biosensors [3,8–10]. Graphene folding is an essential process in the design and manufacturing of graphene origami, and also plays an influential role in its functional mechanical and electrical properties [11]. Even though folding in graphene has been observed extensively in experiments, quantitative investigation of graphene folding has mostly been pursued using

theoretical and computational techniques [3,5,12–14]. Quantitative experimental studies reported in the literature remain quite limited, and cover mostly passive and simple folding deformations along a single folding line [15–19]. Active and controllable folding of graphene with multiple folding lines [20], which is of importance in the pursuit of graphene origami with intricate geometries, remains a challenging issue, in particular at a single graphene sheet level. In this paper, we present a nanomechanical study of z-shape or accordion folding of graphene on a flat substrate by using atomic force microscopy (AFM) techniques. The quantitative AFM measurements in conjunction with nonlinear mechanics modeling and molecular dynamics (MD) simulations reveal that a buckling-driven delamination of graphene occurs in its early-stage folding process, which enables graphene to further deform into a stable self-folded z-shape conformation. The research findings are useful to the study of active and controllable folding of graphene and in the pursuit of graphene origami with complex geometries.

* Corresponding authors.

E-mail addresses: xqwang@uga.edu (X. Wang), cke@binghamton.edu (C. Ke).

2. Results and discussion

2.1. Nanomechanical folding of graphene by using atomic force microscopy

Fig. 1(a) illustrates the AFM-based nanomechanical folding scheme, in which an AFM operates in a lateral force mode. A pre-calibrated AFM cantilever is controlled to laterally slide onto a graphene sheet, which stays on top of a flat substrate, with a specified compressive normal load. The resulting lateral collision force is obtained through measuring the torsional deflection of the AFM cantilever using a laser reflections scheme [21]. The conformational change of the graphene is identified from the recorded AFM topography and lateral force profiles. The AFM measurements were performed inside a Park Systems XE-70 AFM with closed-loop piezo stages. Silicon AFM probes with a nominal tip radius of 10 nm were employed. The normal spring constants of all employed AFM cantilevers were calibrated using thermal tuning methods [22], and found to be within the range of 0.09–0.25 N/m. Their lateral photo-sensitivities were calibrated using two-slope wedge methods [23] and found to be within the range of 0.039–0.11 nN/mV. Graphene sheets employed in this study were obtained through mechanically exfoliating highly ordered pyrolytic graphite (HOPG) films [1].

Fig. 1(b) shows a representative graphene film that was deposited onto a flat silicon oxide substrate. The graphene sample was composed of two partially overlapping graphene sheets. Their heights on the substrate are approximately of the same value, 1.55 nm, as measured from the AFM cross-section profile A–A' shown in the bottom plot in Fig. 1(b). The thickness of the top sheet is measured to be about 1.08 nm with respect to the bottom one. Both sheets are identified as trilayer graphene that has a theoretical thickness of 1.02 nm [15,16]. The nanomechanical folding of the graphene film was performed in a two-step process through controlling the scan starting position and distance of the AFM tip, as well as the applied compressive normal load P_N . The graphene folding conformations after each of the folding step are exhibited in the recorded AFM images shown in Fig. 1(c) and (d), respectively. The 3D schematic drawings shown in Fig. 1(e)–(g) illustrate the original and folded graphene conformations, which are constructed based on the respective AFM measurements shown in Fig. 1(b)–(d). For all experiments, the scanning speed of the AFM tip was set as 500 nm/s. During the first folding step, the AFM tip was controlled to repeatedly scan and collide onto the graphene sheet at one of its apexes that has an internal angle of about 81° for a scan distance of 600 nm, as indicated by the blue arrow marked in Fig. 1(b). An increasing normal load that started from 1 nN and increased at an interval of 2–5 nN was applied. Based on the recorded AFM topography profiles, graphene folding occurred when P_N reached 65 nN and its height profile became flat. Its folding conformation was subsequently imaged by using the same AFM tip operating in a contact mode, and is displayed in Fig. 1(c). It can be seen from the cross-section profile B–B' that the graphene sheet undertook a bulged folding conformation

and the folded graphene segment was not in a full contact with the underlying unfolded graphene, as illustrated in Fig. 1(f). The second folding step was intended to flatten the folded graphene through pushing down the bulged portion of the folded graphene segment onto the underlying graphene segment that stayed flat on the substrate. By repeating the same nanomechanical folding process along the green arrow marked in Fig. 1(c) (i.e., the second folding step), more areas of the graphene film were gradually delaminated from the substrate and folded by the AFM tip. The graphene sheet was eventually found to stay in a z-shape or accordion self-folding conformation after $P_N = 70$ nN was applied, as displayed by the AFM image shown in Fig. 1(d). It is noticed from the AFM image in Fig. 1(d) that a small triangular area of the graphene (*fgh*) was folded on top, which is also visible in Fig. 1(c) and exhibited in pink in Fig. 1(f) and (g). The vertical segment *de* in Fig. 1(c) is measured to be 380 nm in length, which matches the length of the folding edge *fg* in Fig. 1(d). These observations indicate (i) that the folding of the small triangular graphene area occurred during the first folding step with segment *de* as its folding edge; and (ii) that the folding edge *de* turned into the folding edge *fg* through both translation and rotation during the second folding step. Analysis further reveals that the folded small triangle graphene shown in Fig. 1(c) has a smaller area than the one shown in Fig. 1(d), which can be explained based on the difference of its orientations at these two folding conformations. The small triangle graphene shown in Fig. 1(d) is in a flattened conformation as illustrated in Fig. 1(g) and its area is measured to be about $0.037 \mu\text{m}^2$. In comparison, the small triangle shown in Fig. 1(c) is merely its projection on the horizontal plane, and its area (about $0.033 \mu\text{m}^2$) is about 11% smaller than its size in the flat conformation due to its oblique orientation, as illustrated in Fig. 1(f). The original position of the folded triangular area is marked in the AFM image in Fig. 1(b) with white dashed lines based on its geometry shown in Fig. 1(d). The original orientation of the folding line *de* in the flat graphene shown in Fig. 1(b) forms an angle of 60° with the flat scan direction of the AFM tip. Flattening of the deformed graphene film occurred during the second folding step. The folding edge *mn* shown in Fig. 1(d) has a substantially lower height than the folding edge *jk* shown in Fig. 1(c) based on the recorded cross-section profile B–B' and C–C'.

We examine the measured AFM line-scanning topography and the corresponding lateral force profiles at various applied load P_N to better understand the two-step graphene folding process. Fig. 2(a) and (b) show a few selected line-scanning topography and lateral force curves of the graphene during the first and second folding steps, respectively. The measurement shows that the AFM-graphene collision site, which corresponds to the jump in the topography profiles in Fig. 2(a), remained largely unchanged initially, and a noticeable shift occurred when P_N reached 15 nN. A higher P_N resulted in a larger shift toward the lateral collision force direction. The lateral force profiles indicate that the peak lateral collision force increased with the increase of the applied normal load. Based on the recorded topography and lateral force profiles shown in

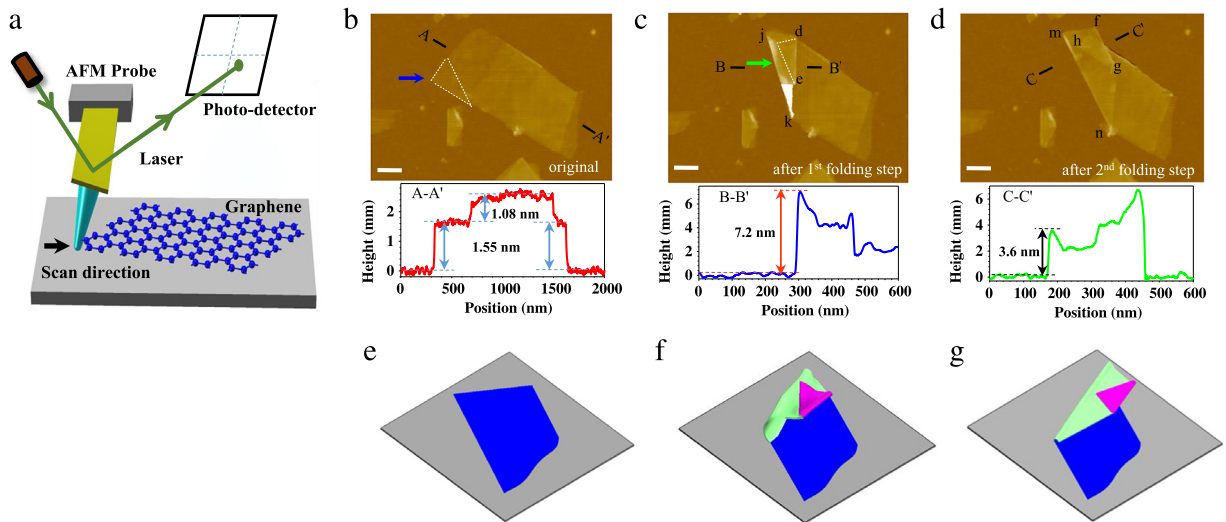


Fig. 1. (a) Schematic of AFM-based nanomechanical folding of graphene on a flat substrate (the drawing is not to scale). (b–d) AFM images of a representative mechanically folded graphene: (b) unfolded graphene; (c) graphene conformation after the first folding step; (d) graphene conformation after the second folding step. The plots below the AFM images are the recorded AFM topography line profiles of the graphene along the respectively marked cross-sections. The white dashed lines are added in (c) to aid in the visualization of the folded triangular graphene. All scale bars represent 200 nm. (e–g) 3D Schematic drawings of the original and folded graphene conformations corresponding to the respective AFM images shown in (b–d). The pink segment stays on top, the blue segment stays flat on the substrate, and the green segment stays in between. (For interpretation of the references to color in this figure legend, the reader is referred to the web version of this article.)

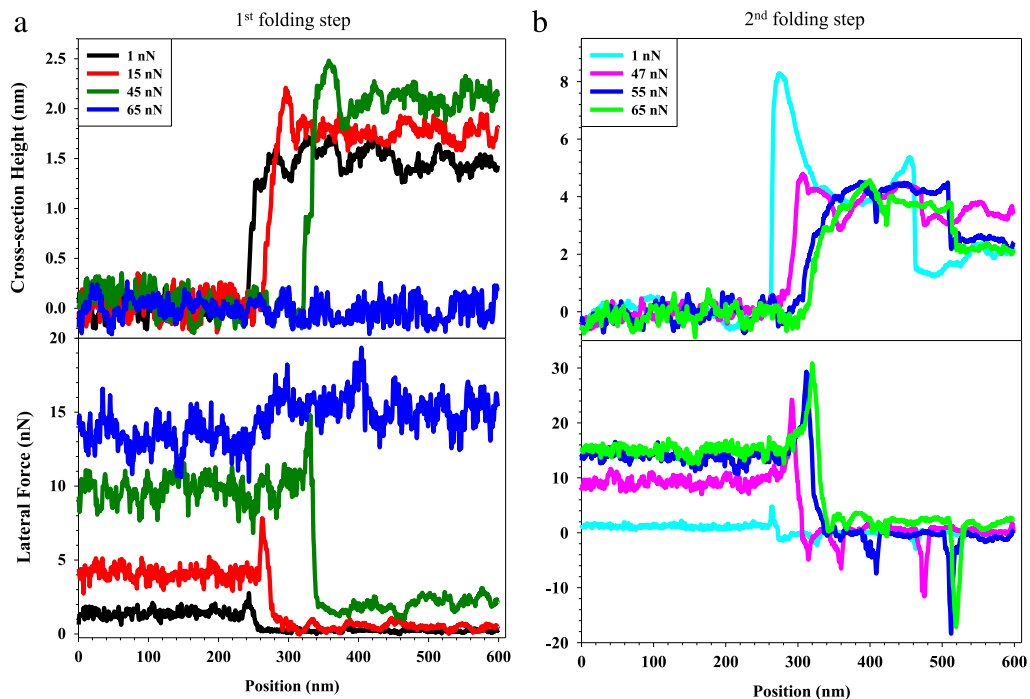


Fig. 2. Selected AFM topography (*top*) and lateral force (*bottom*) line profiles during the first (a) and second (b) folding steps.

Fig. 2(a), it is concluded that an out-of-plane buckling delamination of graphene occurred under the lateral compressive load in the early-stage of the first folding step, as illustrated in the schematic drawing in Fig. 4(a). Our AFM imaging of the graphene after $P_N = 55$ nN was applied (with about 17 nN in the corresponding peak lateral force) during the first folding step, revealed that the

graphene remained at its original position with no visible shape change. This observation indicates that the buckling deformation of the graphene caused by the lateral force was fully reversible, which is consistent with the recorded topography and lateral force curves displayed in Fig. 2(a). The observed continuous shifts of the AFM-graphene collision site with an increasing P_N and the corresponding peak

lateral force indicate that the increasing lateral collision force drove the continuous delamination of the graphene from the substrate, resulting in an increase of the length of the buckled graphene sheet.

The AFM topography and the corresponding lateral force profiles displayed in Fig. 2(b) show the evolution of the graphene folding from the folding line jk to mn during the second folding step. The normal component of the lateral collision force that is perpendicular to the folding line tends to delaminate and push more graphene from the substrate into the folded structure. Its tangent component that is along the folding line orientation leads to a rotation of the folded graphene. The applied normal load P_N results in flattening of the deformed graphene. To the best of our knowledge, *this work is among the first in the quantitative experimental investigation of folding of single graphene sheets with multiple folding lines.*

Even though the z-shape folding experiments presented in Fig. 1(b)–(d) were performed in a two-step manner, it is feasible to turn a flat graphene sheet into a stable self-folded z-shape structure in a one-step folding process, which is demonstrated by the folding experiments displayed in Fig. 3. Fig. 3(a) shows one triangular graphene sheet with an internal angle of about 48° and a thickness of about 3.0 nm, which is composed of approximately 7 graphene layers. The graphene was probed by an AFM tip and folded following the aforementioned folding protocol. Fig. 3(b) shows the folded graphene, which is in a stable self-folded z-shape conformation. The z-shape folding occurred after a *single* AFM scan with a compressive load of 10 nN and a scan distance of 500 nm. The folding experiments displayed in Figs. 1 and 3 clearly demonstrate the potential of the proposed AFM nanomechanical folding technique for manufacturing graphene origami with relatively complex folding geometries in an active and controllable manner.

2.2. Continuum mechanics modeling of delamination driven buckling of graphene

We establish a nonlinear continuum mechanics model to provide insights into the buckling delamination of a triangular-shape graphene on a flat substrate under an in-plane point load. In this model, the graphene is simplified as an inextensible elastic sheet, and is under pure bending deformation. For simplicity, the in-plane load P_L is applied at the apex of the triangular sheet along its angular bisector. The graphene deforms in a buckling delamination mode. The delamination of the graphene is driven by the bending moment at its folding line (also the delamination front) that is in an equilibrium status with the graphene–substrate adhesion interactions. The increasing buckling deformation of the delaminated graphene segment tends to increase the bending moment at its delamination front, resulting in more graphene being delaminated from the substrate and thus an increase of the length of the buckled graphene segment. The folding line of the sheet is perpendicular to the direction of P_L and all the points on the same lines parallel to the folding line have the same bending curvature. Therefore, the buckling deformation of the triangular sheet can be simplified as

a one-dimensional (1D) problem, which is illustrated in Fig. 4(a). It is noted that the bending stiffness of the sheet varies with its width.

Governing equations: The black curve in the bottom illustration of Fig. 4(a) represents the middle-plane deformation of the buckled sheet, which is governed by [12,24]

$$\begin{aligned} \frac{dM}{ds} + V &= 0, & \frac{dV}{ds} + N \frac{d\theta}{ds} &= 0, \\ \frac{dN}{ds} - V \frac{d\theta}{ds} &= 0, \end{aligned} \quad (1)$$

where θ is the rotation angle; s is the arc length measured from point A; M , V and N are the bending moment, shear force and normal force within the sheet, respectively. It is noted that $M = D \cdot w(s) \cdot \kappa = D \cdot w(s) \cdot (d\theta/ds)$, in which D is the per-unit-length bending stiffness of the sheet, $w(s)$ is the width of the sheet and given as $w(s) = 2s \cdot \tan(\alpha/2)$ with α being its internal triangular angle (see Fig. 4(a)), and $\kappa = d\theta/ds$ is its bending curvature. By eliminating V , the second and the third equations in Eq. (1) can be expressed as,

$$\begin{aligned} 2D \cdot \tan\left(\frac{\alpha}{2}\right) \left(s \cdot \frac{d^3\theta}{ds^3} + 2 \frac{d^2\theta}{ds^2} \right) - N \frac{d\theta}{ds} &= 0, \\ 2D \cdot \tan\left(\frac{\alpha}{2}\right) \left[s \cdot \frac{d^2\theta}{ds^2} \frac{d\theta}{ds} + \left(\frac{d\theta}{ds} \right)^2 \right] + \frac{dN}{ds} &= 0. \end{aligned} \quad (2)$$

Boundary conditions: It is noted that $N_B = P_L$, $V_B = R$, $M_B = R \cdot l_{AB}$, where R is the reaction force in the vertical direction at point A, and l_{AB} is the horizontal distance between points A and B. The bending curvature of the sheet at point A is zero, i.e., $\kappa_A = 0$. Position B ($x = l_{AB}$, $y = 0$, $\theta = 0$) is the delamination front, and its bending curvature is given as [25] $\kappa_B = M_B/(D \cdot w(s)) = (2\Gamma_s/D)^{1/2}$, in which M_B is the bending moment at point B and Γ_s is the adhesion energy per unit area between the sheet and the substrate. The total length of the buckled sheet is given as $L_0 = \int_0^{l_{AB}} \sqrt{1 + (dy/dx)^2} dx$.

It is noted that, unlike the problem of bending of a rectangular graphene that has a constant bending rigidity and has been solved analytically [12], the bending of a triangular graphene is governed by highly nonlinear differential equations, which can be only solved numerically. Therefore, the bending curvature of the buckled triangular graphene sheet is obtained numerically through solving the nonlinear differential equations in Eq. (2) with the aforementioned boundary conditions using the Homotopy Perturbation Method (HPM) that is reported in Ref. [26]. For trilayer graphene, $\Gamma_s = 0.338 \text{ J/m}^2$ (Ref. [27]), and $D = 6.92 \text{ eV}$ (Ref. [16]) are employed. It is noted that the sheet width at the triangular apex is set to be 1 nm to avoid the singularity at this point. From an energy point of view, the total energy involved in the out-of-plane buckling delamination of graphene includes the adhesion energy between the delaminated graphene and the substrate and the bending energy stored in the buckled graphene, and equals the work done by the external lateral load. For the triangular sheet as shown in Fig. 4(a), the total energy is given as $E_{tot} = \tan\left(\frac{\alpha}{2}\right) \times L_0^2 \times \Gamma_s + \int_0^{L_0} \frac{Dw(s)}{2} \kappa^2 ds$. It is energetically

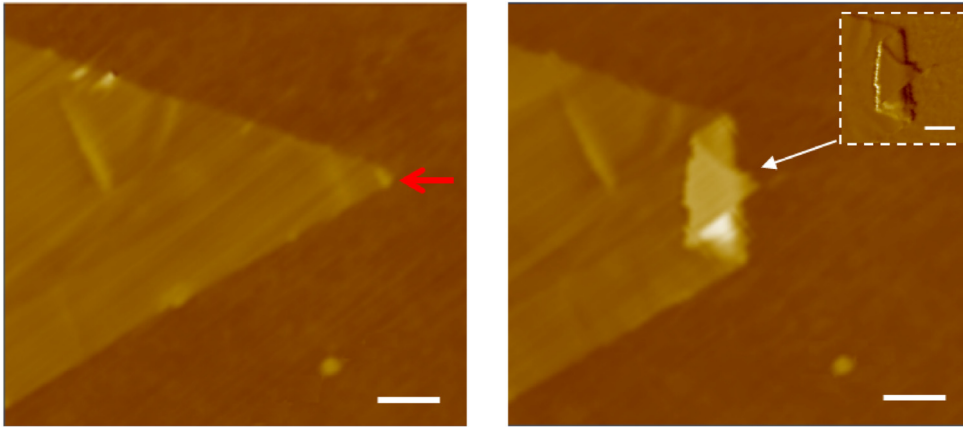


Fig. 3. AFM images of a z-shape folded triangular graphene sheet by using the AFM-based nanomechanical folding approach in a *one-step* folding manner. (Left) The original unfolded graphene. The red arrow indicates the scanning start position and direction of the AFM probe (500 nm in scanning distance). (Right) The z-shape folded graphene (the inset shows the AFM error signal image of the folded graphene region). All scale bars represent 100 nm. (For interpretation of the references to color in this figure legend, the reader is referred to the web version of this article.)

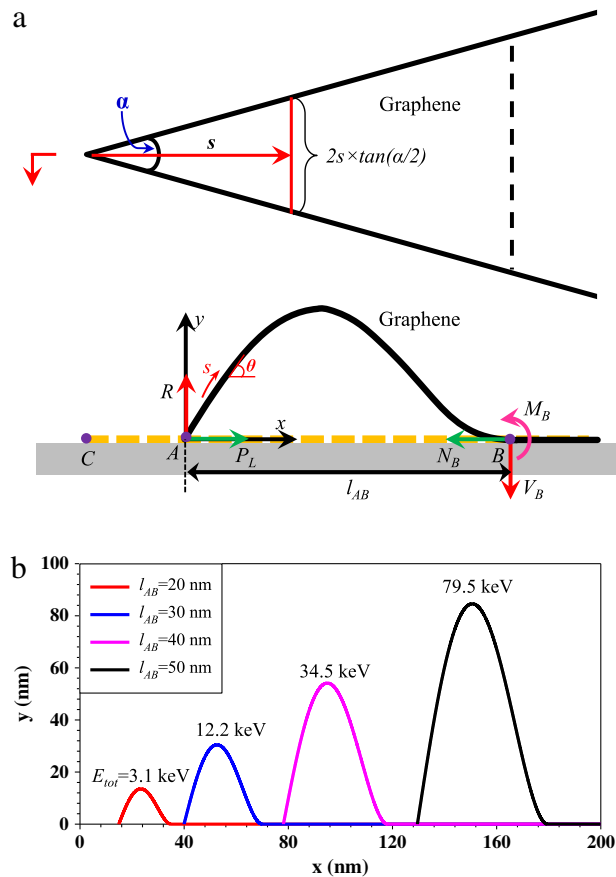


Fig. 4. (a) Schematic of out-of-plane graphene buckling on a flat substrate and the nonlinear continuum mechanics model. The dashed line shows the original position of the flat graphene. (b) Selected buckling deformation profiles of a triangular graphene sheet and their total energies.

favorable to delaminate and buckle a triangular sheet with a smaller internal angle α .

Fig. 4(b) shows four theoretically predicted buckling deformation profiles for a trilayer triangular graphene

sheet with $\alpha = 90^\circ$ based on the continuum mechanics model. The results show that the position of point A continuously shifts towards the external load direction with an increase of l_{AB} , accompanied by increases of

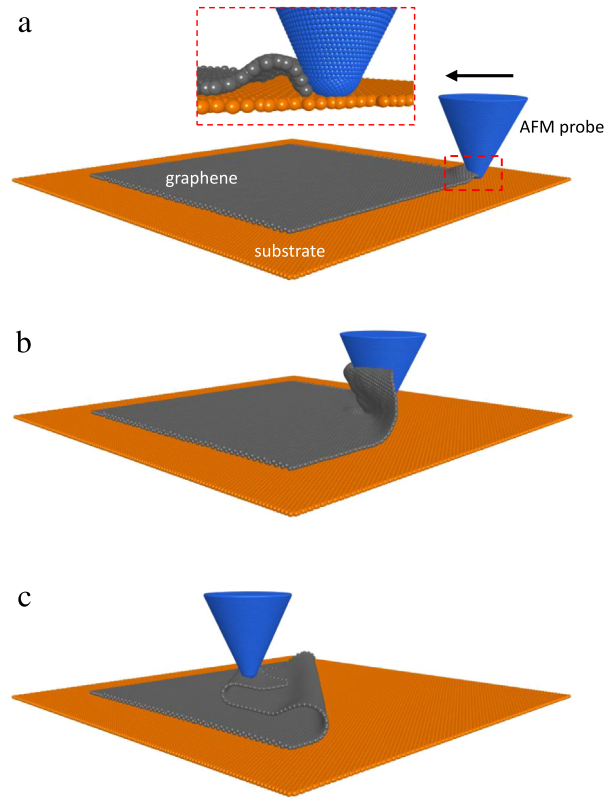


Fig. 5. Selected molecular dynamics simulation snapshots showing the z-folding of a square monolayer graphene sheet on a silicon substrate by using an AFM tip. The black arrow in (a) indicates the moving direction of the AFM tip along the diagonal direction of the square graphene sheet. The image in the dotted-line frame box in (a) is a zoom-in view of the contact region of the AFM tip with the buckled graphene.

the totally buckling length L_0 and the total energy E_{tot} . The results are consistent with the experimental measurements shown in Fig. 2.

2.3. Molecular dynamics simulation of nanomechanical z-shape folding of graphene

We also perform MD simulations to provide insights into the graphene buckling and z-folding processes. In the MD simulations, a cone-shape AFM tip with a tip diameter of 1 nm and a tip height of 5.75 nm is controlled to probe a square monolayer graphene sheet with an edge length of 25 nm that stays on top of a silicon substrate. Monolayer graphene is employed in the MD simulation because its folding process is envisioned to follow the same key folding mechanisms as that of the same-size multilayer graphene, but can be simulated at a much lower computational cost. The MD simulations are performed using AIREBO [28] potentials with a cut-off distance of 8 Å. The AFM tip is originally placed at 0.15 nm above the surface of the substrate, and is controlled to laterally compress the graphene along its diagonal direction at a constant speed of 0.071 nm/ps. The system is relaxed after every 0.2 ps to allow the propagation of the mechanical wave. As the AFM tip approaches to compress the corner of the graphene sheet, the graphene starts to delaminate from the substrate and stays in a buckled conformation, as shown in Fig. 5(a) and the zoom-in view. The rest

portion of the graphene sheet remains intact, which can be ascribed to the strong van der Waals interaction between the graphene sheet and the substrate. As simulations continue, more areas of the graphene are delaminated and buckled, and the deformed graphene starts to fold inward and conform to the AFM tip surface, as displayed in Fig. 5(b). The inward folding is induced by the AFM tip shape [29] and can be considered to reach a more stable crumpling deformation configuration than the buckled configuration where the buckled regions of the graphene sheet adhere together [11,20]. The AFM tip is pulled up by 0.5 nm after reaching the center of the graphene sheet. The continuous lateral compression of the graphene sheet along its diagonal direction leads to the formation of the z-shape folding, as shown in Fig. 5(c). MD simulations show that the graphene is able to maintain its z-shape folding conformation even after removing the AFM tip. The MD simulation results of the graphene delamination/buckling and z-shape folding processes are consistent with our AFM experiments and continuum mechanics modeling results.

The out-of-plane buckling deformation of graphene is an essential process in the formation of its z-shape folding conformation. The graphene buckling enables its further deformation into a crumpled shape before entering a z-shape folding conformation, which may be maintained in a self-folded manner thanks to adhesive interactions between the close-by graphene surfaces. From a manufacturing point view, the z-shape folding approach

based on the buckling of graphene is more efficient than the simple folding-up approach [16,18], by which graphene needs to be folded twice along different sides in order to form the z-shape structure.

3. Conclusion

In summary, we investigate the z-shape nanomechanical folding of originally flat graphene sheets on a flat substrate by using AFM in conjunction with nonlinear continuum modeling and MD simulations. The study reveals that the out-of-plane buckling delamination of graphene occurs in its early-stage folding process, which enables graphene to deform into a stable self-folded z-shape conformation. The results show that it is plausible to turn individual flat graphene sheets into relatively sophisticated structures by using the AFM-based nanomechanical folding approach. These research findings are useful to the study of active and controllable folding of graphene or other 2D nanomaterials, and in the pursuit of their origami with intricate geometries.

Acknowledgments

This work was supported by National Science Foundation under Grant Nos. CMMI-1429176, CMMI-1537333, and CMMI-1306065. The simulations were performed at the Georgia Advanced Computing Resource Center at the University of Georgia.

References

- [1] K.S. Novoselov, A.K. Geim, S.V. Morozov, D. Jiang, Y. Zhang, S.V. Dubonos, I.V. Grigorieva, A.A. Firsov, *Science* 306 (2004) 666.
- [2] C. Lee, X. Wei, J.W. Kysar, J. Hone, *Science* 321 (2008) 385.
- [3] S. Zhu, T. Li, *ACS Nano* 8 (2014) 2864.
- [4] M. Beeton, L. Zhang, X. Wang, *Chem. Phys. Lett.* 584 (2013) 135.
- [5] L. Zhang, X. Zeng, X. Wang, *Sci. Rep.* 3 (2013).
- [6] V.B. Shenoy, D.H. Gracias, *MRS Bull.* 37 (2012) 847.
- [7] M.K. Blees, A.W. Barnard, P.A. Rose, S.P. Roberts, K.L. McGill, P.Y. Huang, A.R. Ruyack, J.W. Kevek, B. Kobrin, D.A. Muller, P.L. McEuen, *Nature* 524 (2015) 204.
- [8] J. Zang, C. Cao, Y. Feng, J. Liu, X. Zhao, *Sci. Rep.* 4 (2014) 6492.
- [9] F.H.L. Koppens, T. Mueller, P. Avouris, A.C. Ferrari, M.S. Vitiello, M. Polini, *Nat. Nanotechnol.* 9 (2014) 780.
- [10] G. Zeng, Y. Xing, J. Gao, Z. Wang, X. Zhang, 2010.
- [11] T. Al-Mulla, Z. Qin, M.J. Buehler, *J. Phys.: Condens. Matter* 27 (2015) 345401.
- [12] X. Meng, M. Li, Z. Kang, X. Zhang, J. Xiao, *J. Phys. Appl. Phys.* 46 (2013) 055308.
- [13] S. Cranford, D. Sen, M.J. Buehler, *Appl. Phys. Lett.* 95 (2009) 123121.
- [14] Z. Zhou, D. Qian, V.K. Vasudevan, R.S. Ruoff, *Nano Life* (2012).
- [15] X. Chen, L. Zhang, Y. Zhao, X. Wang, C. Ke, *J. Appl. Phys.* 116 (2014) 164301.
- [16] X. Chen, C. Yi, C. Ke, *Appl. Phys. Lett.* 106 (2015) 101907.
- [17] K. Kim, Z. Lee, B.D. Malone, K.T. Chan, B. Alemán, W. Regan, W. Gannett, M.F. Crommie, M.L. Cohen, A. Zettl, *Phys. Rev. B* 83 (2011) 245433.
- [18] H.C. Schniepp, K.N. Kudin, J.-L. Li, R.K. Prud'homme, R. Car, D.A. Saville, I.A. Aksay, *ACS Nano* 2 (2008) 2577.
- [19] J. Zhang, J. Xiao, X. Meng, C. Monroe, Y. Huang, J.-M. Zuo, *Phys. Rev. Lett.* 104 (2010) 166805.
- [20] J. Zang, S. Ryu, N. Pugno, Q. Wang, Q. Tu, M.J. Buehler, X. Zhao, *Nature Mater.* 12 (2013) 321.
- [21] X. Chen, M. Zheng, C. Park, C. Ke, *Appl. Phys. Lett.* 102 (2013) 121912.
- [22] C.T. Gibson, G.S. Watson, S. Myhra, *Scanning* 19 (1997) 564.
- [23] D.F. Ogletree, R.W. Carpick, M. Salmeron, *Rev. Sci. Instrum.* 67 (1996) 3298.
- [24] Y. Mikata, *J. Nanomech. Micromech.* 3 (2013) 04013004.
- [25] Y. Zhao, X. Chen, C. Park, C.C. Fay, S. Stupkiewicz, C. Ke, *J. Appl. Phys.* 115 (2014) 164305.
- [26] J.-H. He, *Internat. J. Non-Linear Mech.* 35 (2000) 37.
- [27] S.P. Koenig, N.G. Boddeti, M.L. Dunn, J.S. Bunch, *Nat. Nanotechnol.* 6 (2011) 543.
- [28] S.J. Stuart, A.B. Tutein, J.A. Harrison, *J. Chem. Phys.* 112 (2000) 6472.
- [29] Y. Dong, X.Z. Liu, P. Egberts, Z. Ye, R.W. Carpick, A. Martini, *Tribol. Lett.* 50 (2012) 49.